Quantum dynamics of bond breaking in a dissipative environment: Indirect and direct photodesorption of neutrals from metals

Peter Saalfrank
Institut für Physikalische und Theoretische Chemie, Freie Universität Berlin, Takustrasse 3, D-14195 Berlin, Germany

Ronnie Kosloff
Department of Physical Chemistry and the Fritz-Haber Research Center for Molecular Dynamics, The Hebrew University, Jerusalem 91904, Israel

(Received 9 April 1996; accepted 26 April 1996)

The dynamics of uv/visible laser-induced nonthermal desorption of neutral molecules from metal surfaces are studied by Liouville–von Neumann equations for quantum open systems. A one-dimensional, two-state Gadzuk–Antoniewicz model is adopted, representative for NO/Pt(111). Electronic quenching due to coupling of the adsorbate negative ion resonance to the metal electrons is treated within the Lindblad dynamical semigroup approach. Both indirect (hot-electron mediated) and hypothetical direct (dipole) excitation processes are considered. For the indirect pathways, DIET (single-excitation) and DIMET (multiple-excitation) limits are studied using one- and double-dissipative channel models, respectively. To reproduce experimental desorption yields and desorbate translational energies, we estimate the quenching lifetime for NO/Pt(111) to be less than 5 fs. We also extend previous quantum treatments of photodesorption processes to the case of coordinate-dependent quenching rates. Further, the characteristic scaling laws of desorption yields versus laser fluence are derived for each of the individual excitation pathways. Finally, the possibility to control photoreactivity at surfaces by different, vibration-promoted schemes (surface heating, ir+uv two-photon strategies, use of pulsed uv lasers) is examined. © *1996 American Institute of Physics.* [S0021-9606(96)02529-9]

I. INTRODUCTION

Quantum dynamics of elementary processes taking place at the gas–solid interface is of fundamental importance. These processes include electronically adiabatic events such as surface-assisted dissociation of H_2 molecules prepared in molecular beams,[1] as well as probably nonadiabatic processes such as direct dissociation of heavier diatomics,[2,3] and uv/visible-laser induced adsorbate photodesorption, photodissociation, and photoreaction.[4,5] Photochemistry in particular on metals is characterized by the possibility to enforce the initial (adsorbate) electronic excitation not only *directly*, i.e., through an allowed dipole transition, but also in an *indirect* fashion, i.e., through ''hot'' substrate electrons. Further, these excitations typically survive only for very short periods, ranging from nanoseconds for insulator substrates down to femtoseconds for metals.

In the present study, we focus on the desorption of neutral molecules (like NO) from metal surfaces [like Pt(111)]. For NO/Pt(111), where ns-laser induced photodesorption could be experimentally confirmed,[6] the excitation is believed to be of the indirect type. Specifically, uv/visible-laser absorption creates hot metal electrons (electron hole pairs) which, when resonant with low-lying empty adsorbate levels, form a ''negative ion resonance.'' The excess electrons tunnel back into the substrate typically on a fs time scale, and most of the energy gained dissipates away. However, a small fraction of the absorbed electromagnetic field energy may have been temporarily trapped in the molecule–surface bond, to break it eventually.

This scenario, as well as possible similar ones can be described within the Antoniewicz variant[7] of the well-known Menzel–Gomer–Redhead (MGR) model[8] of **d**esorption **i**nduced by **e**lectronic **t**ransitions (DIETs). Accordingly, the initial excitation which is understood as a Franck–Condon transition can be induced by, e.g., photons (PSD), electrons (ESD) or by direct dipole or indirect hot-electron coupling. This transition is from a bound ground state potential $\hat{V}_g(Z)$ to a repulsive (MGR) or image-charge stabilized bound (Antoniewicz) state $\hat{V}_e(Z)$ (where Z is, apart from a possible shift, the distance between the molecule and the surface). ''Upstairs,'' the adsorbate moves away from (MGR) or towards (Antoniewicz) the surface, relaxes back to $\hat{V}_g(Z)$ by the relevant quenching process, and desorbs often with low probability—if only enough kinetic (MGR) or potential (Antoniewicz) energy has been gained. For NO/Pt(111), an Antoniewicz-type model has been designed by Gadzuk *et al.*[9,10]

A characteristic feature of DIET is the occurrence only of single excitations. For indirect excitation mechanisms, this situation typically emerges from the use of ns lasers, which for all theoretical purposes can be considered as continuous wave (cw) light sources. These produce only a small concentration of hot carriers, and subsequent excitations of the molecule–surface bond are rare on the time scales of adsorbate vibrational relaxation, and are therefore uncorrelated. In contrast, as emphasized by Misewich *et al.*,[11] the use of fs- to ps-pulsed light should make multiple-excitations possible. Under these conditions a high-density hot-electron gas is cre-

ated in the metal, rapidly thermalizing to give a sharply peaked electronic temperature profile $T_{el}(t)$. Typically several thousands Kelvin peak temperature is obtained. With respect to desorption yields, this so-called **d**esorption **i**nduced by **m**ultiple **e**lectronic **t**ransitions (DIMETs) was found to be much more efficient than the DIET process. The scaling with laser fluence obeys a power law rather than a linear relation as for DIET. For NO/Pd(111), it was also found that DIMET desorbates are translationally colder[11] than the corresponding DIET products.

On the theoretical side, numerous descriptions have been applied to these processes such as classical treatments,[11–15] semiclassical,[9,10,16,17] time-independent quantum,[18,19] or time-dependent quantum descriptions.[15,20–30] In several of these studies not only one-dimensional, two-state MGR- or Antoniewicz-type models have been adopted. Rather, rotational,[12,13,20] vibrational,[9,10,14,15,21,24,25,29,30] or frustrated translational[26] adsorbate degrees of freedom were considered as well. Also, multiple-state models,[18,22,27] or those which take the continuum of substrate electronic excitations in some other way into account,[23] have been proposed. Among the systems studied are H,O/W,[16] O/Pd(111),[17] NO/Ag(111),[12] NO/Pt(111),[9,10,20,23,25,27,28,30] NO/Pd(111),[11] NO, CO/NiO,[13] CO/Pt(111),[20] NH_3/Pt(111),[21] NH_3/Cu(111),[14,15,24,29,30] and Kr,Ar,N_2O/Ru(100).[26]

All of these theoretical approaches are confronted with two basic problems, namely (1) the microscopic modeling of the excitation and quenching processes, and (2) the proper inclusion of dissipation into the (quantum) dynamics calculations. Though multiple-state models[18,22,27] or the explicit inclusion of electronic degrees of freedom[23] point to the key role played by (electronic) nonadiabaticity, in practice mostly a semiphenomenological approach is adopted, in which a phenomenological electronic quenching rate is chosen to fit selected experimental observables. This approach will be followed here also. If thermal hot-electron excitation dominates, an assumed excited state lifetime automatically fixes also the excitation rate through *microscopic reversibility* or *the principle of detailed balance*.

The proper inclusion of dissipation, in particular of the *continuous* electronic quenching, has been tried in several ways. One of them is the use of imaginary potentials in ordinary, two-state nuclear Schrödinger equations,[16,20,27] another one the explicit inclusion of the electron motion.[23] Alternatively, Gadzuk suggested to run different quantum wave packets corresponding to different *residence times* τ_R on an excited state surface, and subsequently to incoherently average over individual operator expectation values $\langle \hat{A}(\tau_R) \rangle$ with a weighting function $e^{-\tau_R/\tau}$. This procedure was introduced to simulate an exponential decay of the resonance.[9,10]

We recently suggested to employ density matrices rather than wave packets, and to solve Liouville–von Neumann equations for quantum open systems rather than Schrödinger equations.[31] There is a connection between the wave function and the density matrix ansatz, though, as shown by several workers in the quantum optics community.[32] Namely, the Liouville–von Neumann equations can be solved exactly by *stochastic wave packet methods* (i.e., by repeated solutions of Schrödinger equations with non-Hermitean Hamiltonians rather than by direct density matrix propagation) if the dissipative part of the open system LvN equation is of the so-called Lindblad[33] form. With this in mind it can be shown[34] that the Gadzuk approach is actually equivalent to a special LvN equation, namely, one in which only the deexcitation dynamics are considered, and in which the quenching rate is coordinate independent. However, Gadzuk's scheme is not generally applicable to the cases to be considered below (multiple-dissipative channels, coordinate-dependent quenching, direct and indirect excitation). Further, in the present applications desorption probabilities are low, and therefore the ordinary and more generally applicable Monte Carlo stochastic wave packet approaches cannot be used economically either.[34] Therefore, in this work the numerical techniques outlined in Ref. 31, i.e., direct density matrix propagation using a polynomial expansion for the time-evolution superoperator,[35] and grid representation of all operators[36] will be adopted.

The plan of the paper is as follows. We first recapitulate the dissipative photodesorption models developed in Ref. 31, and the numerical techniques used (Secs. II and III). This gives us also the opportunity to provide more details than previously, and to extend the earlier formalism in several ways. First, the theory will be generalized to the case of coordinate-independent quenching. Second, besides (indirect) DIET and DIMET we will show how to treat direct (dipole) excitation. Third, an algorithm to perform an asymptotic kinetic energy analysis within the density matrix approach will be proposed. In Sec. IV, we focus on the desorption dynamics in the single-excitation (DIET) limit, and try to estimate a realistic quenching lifetime for NO/Pt(111). We will also study effects associated with coordinate-dependent quenching rates. In Secs. V and VI, possible DIMET and (hypothetical) direct excitation scenarios (using pulsed lasers) are considered. The scaling of the desorption yields with laser fluence, and the kinetic energies of the desorbing particles will be used as signatures for the various excitation mechanisms. In Sec. VII various possibilities to actively control desorption yields in the presence of strong dissipation will be discussed. A final Sec. VIII concludes our work.

II. MODELS FOR POTENTIALS, DISSIPATION, AND EXCITATION

A. Potentials and Hamiltonian

In our treatment of the photostimulated desorption of NO from Pt(111) we adopt the one-dimensional, two-state model suggested by Gadzuk.[9,10] For the ground state potential energy curve (PEC) we write

$$\hat{V}_g(Z) = D[1 - e^{-\alpha Z}]^2 \tag{2.1}$$

with Z being the deviation of the molecule's center of mass from the equilibrium adsorbate–surface distance. D and α are the Morse well depth and exponent, respectively, with parameters given in Table I.

For the excited, negative ion resonance state $\hat{V}_e(Z)$, the following parametrization is used:

TABLE I. Computational parameters for (i) potential, (ii) time propagation and absorber, (iii) grid and cutoff function $\hat{f}(Z)$ [Eq. (2.30)], (iv) hot-electron temperature profile $T_{el}(t)$ [Eq. (2.18)], and electric field coupling [Eq. (2.21)].

Potential parameters			
Ground state		Excited state	
D	0.039 69 hartree	$Z_{\rm im}$	1.757 a_0
α	1.708 a_0^{-1}	ϵ	0.183 75 hartree
		δe	1
Propagation and absorber			
Propagation		Absorber	
Δt	1.00 fs	V_0	0.02 hartree
Pol. order M	16	β	10 a_0^{-1}
T	500 fs	Z_e	+18.44 a_0
Grid and cutoff function			
Grid		Cutoff function	
Z_0	−2.00 a_0	Z_d	+4.00 a_0
Δ	0.04 a_0	γ	5 a_0^{-1}
L	512		
DIMET and direct parameters			
DIMET		Direct	
T_s, T_m	Variable	$\mu_{eg}E_0$	Variable
τ_1	194 fs	$\hbar\omega$	0.056 hartree
τ_2	15 fs	σ	48 fs
τ_3	3.6 fs	t_p	109 fs

$$\hat{V}_e(Z)=\hat{V}_g(Z)-\frac{(\delta e)^2}{4(Z-Z_{\rm im})}+\epsilon. \tag{2.2}$$

Here, the last term accounts for the proper asymptotics $\{\lim_{Z\to+\infty}[\hat{V}_e(Z)-\hat{V}_g(Z)]=\epsilon=\phi-\mathrm{EA}$, with ϕ being the work function of Pt(111), and EA the adsorbate electron affinity$\}$. The second term accounts for the image charge stabilization of $\hat{V}_e(Z)$. ($Z_{\rm im}$ is the location of the image plane relative to the ground state equilibrium geometry, δe the fraction of charge transferred.) The parameters occurring in Eq. (2.2) are also given in Table I.

Note that the potential curves differ somewhat from the ones employed in Refs. 27 and 31, and are more similar to those of Refs. 9 and 10. With the new potential parameters, the vertical excitation energy $|g\rangle\to|e\rangle$ becomes ≈1.5 eV (previously ≈2.5 eV), and fits now the experimental estimate.[37]

The two-state system Hamiltonian is written as

$$\hat{H}=\hat{H}_e|e\rangle\langle e|+\hat{H}_g|g\rangle\langle g|+\hat{V}_{eg}|e\rangle\langle g|+\hat{V}_{ge}|g\rangle\langle e|, \tag{2.3}$$

where in the one-dimensional model

$$\hat{H}_n=-\frac{\hbar^2}{2\mu}\frac{\partial^2}{\partial Z^2}+\hat{V}_n(Z);\quad n=g,e; \tag{2.4}$$

and where for NO/Pt(111), $\mu=m_{\rm NO}$. Further, $|n\rangle$ denotes the individual electronic states, and the terms $\hat{V}_{eg}|e\rangle\langle g|$ and $\hat{V}_{ge}|g\rangle\langle e|$ (with $\hat{V}_{eg}=\hat{V}_{ge}^*$) induce possible *direct* (e.g., dipole) transitions from $|g\rangle$ to $|e\rangle$ and vice versa (see below).

B. Dissipation

To include dissipation, such as electronic quenching or the hot-electron mediated indirect excitation in the DIMET case, we solve general Liouville–von Neumann equations for quantum open systems,

$$\mathscr{L}\hat{\rho}=\dot{\hat{\rho}}=-\frac{i}{\hbar}[\hat{H},\hat{\rho}]+\dot{\hat{\rho}}_D=\mathscr{L}_H\hat{\rho}+\mathscr{L}_D\hat{\rho} \tag{2.5}$$

giving the change in time of the *reduced nuclear density matrix* $\hat{\rho}$. For later use, we have also introduced the total, Hamiltonian, and dissipative Liouvillian superoperators $\mathscr{L}$, $\mathscr{L}_H$, and $\mathscr{L}_D$, respectively. In the two-state case, the density operator is

$$\hat{\rho}=\hat{\rho}_{ee}|e\rangle\langle e|+\hat{\rho}_{gg}|g\rangle\langle g|+\hat{\rho}_{eg}|e\rangle\langle g|+\hat{\rho}_{ge}|g\rangle\langle e|, \tag{2.6}$$

with $\hat{\rho}_{nm}=\langle n|\hat{\rho}|m\rangle_{\rm el}$ $(n,m=g,e)$ being the elements of the density operator expressed in the electronic basis, which are still operators in configuration space. (In the following, ''configuration space,'' ''grid,'' and ''coordinate space'' will be used interchangeably; further, $\langle\ \rangle_{\rm el}$ denotes integration over electronic coordinates.)

The first term on the r.h.s. of Eq. (2.5) is the *Hamiltonian* part, describing the conservative time evolution of the (reduced) system modes. This term also accounts for the direct processes induced by an external electromagnetic field. The second term on the r.h.s. of Eq. (2.5) is the *dissipative* part, accounting for all environmental effects, and for all neglected degrees of freedom.

There is an ongoing dispute of how to choose the actual form of $\mathscr{L}_D\hat{\rho} = \dot{\hat{\rho}}_D$. Even if the Markov approximation is made,

$$\dot{\hat{\rho}}_D(t) = F[\hat{\rho}(t)], \tag{2.7}$$

several possibilities remain. One popular line of research emerges from a system–bath formalism, in which the environment is treated as a collection of unobserved modes, only weakly coupled to the system. This allows among other approximations the use of perturbation theory, and leads, after tracing out the bath modes, to what is commonly referred to as the ''Redfield theory.''[38] In the Redfield equations of motion, individual density matrix elements are dissipatively coupled through the Redfield tensor (a structure containing N^4 elements if $N\times N$ is the dimension of the density matrix). Redfield theory is known to violate *complete positivity*, which makes it impossible to generally interpret the diagonal elements of the density matrix as probabilities.[39,40] (They can become negative.)

A more phenomenologically oriented approach, which preserves complete positivity by construction, is the *dynamical semigroup* formalism of Lindblad[33] and others.[41] Here,

$$\dot{\hat{\rho}}_D = \mathscr{L}_D\hat{\rho} = \sum_{k=1}^{K} (\hat{C}_k\hat{\rho}\hat{C}_k^+ - \tfrac{1}{2}[\hat{C}_k^+\hat{C}_k, \hat{\rho}]_+), \tag{2.8}$$

with $\hat{C}_k$ being the positive semidefinite ''Lindblad operators,'' which determine ''what'' dissipates ''how fast'' in each of the K dissipative channels k. $[\ ]_+$ denotes an anticommutator. Here, k can label electronic or vibrational energy relaxation (T_1 processes), pure electronic or vibrational dephasing (T_2 processes), momentum diffusion[32] or phase fluctuations in an external electromagnetic field.[42] The Lindblad operators are usually chosen to fit selected experimental data, e.g., spectroscopical linewidths.

The restriction to selected types of dissipation makes the Lindblad approach potentially quite economical, but inherently a semiempirical theory. However, as shown, for instance, in Ref. 43, the dynamical semigroup approach is fully compatible with microscopic relaxation models—the only requirement is the positive semidefiniteness of the relaxation operators. As shown previously by Tannor *et al.* for a damped harmonic quantum oscillator, the semigroup approach destroys translational invariance, i.e., leads to coordinate-dependent friction (as does the Redfield theory if the so-called secular approximation is made).[40] Although this may generally be problematic, in the present case (electronic) friction should in fact decrease with increasing molecule–surface distance. Further, Redfield-type theories could be disastrous if applied to photodesorption of neutrals from metals, where the relevant probabilities are typically small and a strict probabilistic interpretability of the density matrix is required.

The processes to be considered below are ultrafast ($t_{\text{process}}<1$ ps). Therefore, we only consider electronic energy relaxation and neglect vibrational dissipation for the moment. Also, pure dephasing effects are not studied here.

C. Three specific photodesorption models

1. Indirect single-excitation (DIET) model

In the single-excitation (DIET) model we assume that the initial excitation is an impulsive, Franck–Condon type transition from $|g\rangle$ to $|e\rangle$. The initial state is taken to be

$$\hat{\rho}(0) = \hat{\sigma}|e\rangle\langle e|. \tag{2.9}$$

Here, $\hat{\sigma}$ is the pre-excitation (ground state) density operator, derived from the (bound) vibrational states $|v_g\rangle$ on $\hat{V}_g$,

$$\hat{H}_g|v_g\rangle = \epsilon_{vg}|v_g\rangle; \quad v=0,\ldots,N-1 \tag{2.10}$$

according to

$$\hat{\sigma} = \sum_v w_v|v_g\rangle\langle v_g|. \tag{2.11}$$

We consider both *pure* states with

$$w_v = \delta_{vv'}, \tag{2.12}$$

and *thermal* (mixed) states, for which

$$w_v = \frac{\exp\left\{-\dfrac{\epsilon_{vg}}{k_BT_s}\right\}}{\mathrm{tr}\left\{\exp\left\{-\dfrac{\hat{H}_g}{k_BT_s}\right\}\right\}} \tag{2.13}$$

is the Boltzmann weight of state $|v_g\rangle$ with energy ϵ_{vg} at surface temperature T_s.

Once on $\hat{V}_e$, the nuclear density time evolves and is simultaneously continuously backtransferred to $|g\rangle$ through quenching. The quenching, i.e., the coupling of the excited adsorbate state to a continuum of metal electronic excitations, is modeled by choosing a *spontaneous emission* Lindblad operator $\hat{C}_1$ of the form

$$\hat{C}_1 = \sqrt{\hat{\Gamma}_{ge}}|g\rangle\langle e|. \tag{2.14}$$

In Eq. (2.14), $\hat{\Gamma}_{ge}$ is a quenching rate (of dimension time^{-1}), which is chosen to fit the experimentally estimated desorption yield *per excitation event* for NO/Pt(111)[6] (see below). Note that in general $\hat{\Gamma}_{ge}$ is an operator in coordinate space. The present treatment of DIET is in full analogy to most of the earlier wave packet or classical approaches.[8]

2. Indirect multiple-excitation (DIMET) model

In the multiple-excitation (DIMET) model we start with the adsorbate in its electronic ground state,

$$\hat{\rho}(0) = \hat{\sigma}|g\rangle\langle g|, \tag{2.15}$$

and $\hat{\sigma}$ given by Eq. (2.11).

Other than in the DIET case, the indirect excitation step is explicitly included. The hot-electron mediated excitation can be treated as dissipation and is modeled here by a Lindblad operator $\hat{C}_2$ of the form

$$\hat{C}_2 = \sqrt{\hat{\Gamma}_{eg}(t)}|e\rangle\langle g|. \tag{2.16}$$

In Eq. (2.16), $\hat{\Gamma}_{eg}(t)$ is the rate with which nuclear density is transferred from $|g\rangle$ to $|e\rangle$. It is a coordinate- and explicitly

time-dependent operator. Both dependences follow from the principle of detailed balance, which relates $\hat{\Gamma}_{eg}$ to $\hat{\Gamma}_{ge}$ by

$$\hat{\Gamma}_{eg}(Z,t)=\hat{\Gamma}_{eg}(Z)\cdot\exp\left\{-\frac{\hat{V}_e(Z)-\hat{V}_g(Z)}{k_B T_{\rm el}(t)}\right\}. \tag{2.17}$$

Equation (2.17) expresses the fact that both excitation and quenching are due to the same physical process (coupling of adsorbate excited states to metal electronic excitations), and shows that the coordinate dependence of $\hat{\Gamma}_{eg}(Z)$ emerges from two sources, namely (1) from the possible coordinate dependence of the quenching, and (2) from the energy difference $\hat{V}_e(Z)-\hat{V}_g(Z)$. The time dependence arises from the fact that we model a pulsed laser experiment, giving rise to a time-dependent electronic temperature $T_{\rm el}(t)$. $T_{\rm el}(t)$ can be calculated semimicroscopically within a coupled diffusion model from the laser (fluence, pulse width) and substrate characteristics (electron and phonon heat capacities, thermal conductivity, electron–phonon coupling constant).[44] In this work, we rather use a model form suggested in Ref. 44,

$$T_{\rm el}(t)=T_m\cdot\frac{e^{-t/\tau_1}}{e^{-t/\tau_2}+1}\cdot g(t), \tag{2.18}$$

where $g(t)$ is a smoothing cutoff function, which we take to be

$$g(t)=1-\frac{1}{\exp\{(t-\tau_2)/\tau_3\}+1}. \tag{2.19}$$

In Eq. (2.18), T_m is related (but, due to the cutoff function, not exactly equal) to the peak electronic temperature $T_{\rm max}$, and τ_1 and τ_2 are two characteristic times, related to the characteristic variation of $T_{\rm el}(t)$, and the laser pulse width, respectively. Effects associated with finite phonon temperatures T_s are not considered in Eq. (2.18). The parameters used in Eqs. (2.18) and (2.19) can be found in Table I.

In our DIMET model the energy-delivering excitation process (2.16) competes with the stationary, energy-consuming quenching process (2.14). By using Eqs. (2.14) and (2.16) we describe in essence electron transfer processes, but we do not make any (Fermi–Dirac) statistical corrections connected with the spin-1/2 nature of the electrons.

3. Direct (dipole) excitation model

In the direct (dipole) excitation model it is assumed that the explicitly included excitation is due to dipole coupling between $|g\rangle$ and $|e\rangle$, and that the heating of the metal electronic system is negligible. This excitation pathway may not play a major role for NO/Pt(111), but is important for other systems.[45] This justifies the investigation of the direct mechanism within a model study.

In the direct excitation model we start from the ground state, and use the initial density operator $\hat{\rho}(0)$ defined in Eq. (2.15). Quenching is again achieved with the spontaneous emission Lindblad operator $\hat{C}_1$ defined in Eq. (2.14). The direct excitation of the molecule–surface bond is modeled within the Hamiltonian part of the LvN equation (2.5) by using the semiclassical dipole coupling operator in Eq. (2.3)

$$\hat{V}_{eg}=-\hat{\mu}_{eg}(Z)\cdot E_z(t). \tag{2.20}$$

Here, $\hat{\mu}_{eg}(Z)$ is the (z component) of the (Z dependent) electronic transition dipole moment operator, and $E_z(t)$ is the z component of the external electromagnetic field. Also in the direct excitation scenario we wish to model a pulsed laser experiment. Hence we choose

$$E_z(t)=E_0\cdot\cos\,\omega t\cdot\exp\left\{-\left(\frac{t-t_p}{\sigma}\right)^2\right\}, \tag{2.21}$$

with the field amplitude E_0, the field frequency ω, the (Gaussian) pulse peak time t_p, and the pulse width σ. We will further assume $\hat{\mu}_{eg}=\mu_{eg}=$const. (Condon approximation), and absorb the actual (unknown) value of the constant in the prefactor E_0 to Eq. (2.21). The parameters actually used are listed in Table I.

D. Computation of properties

1. General

Properties of interest, i.e. expectation values of quantum mechanical operators $\hat{A}$ are calculated here from

$$\langle\hat{A}\rangle(t)={\rm tr}\{\hat{A}\hat{\rho}(t)\}. \tag{2.22}$$

Performing the trace in the electronic basis and using the appropriate expansion for $\hat{A}$ we get ($\hat{A}_{nm}=\langle n|\hat{A}|m\rangle_{\rm el}$)

$$\langle\hat{A}\rangle(t)={\rm tr}\{\hat{A}_{ee}\hat{\rho}_{ee}+\hat{A}_{eg}\hat{\rho}_{ge}+\hat{A}_{ge}\hat{\rho}_{eg}+\hat{A}_{gg}\hat{\rho}_{gg}\}, \tag{2.23}$$

where the trace in Eq. (2.23) will be evaluated in the configuration space representation (see below).

2. State populations, energy, and desorption probability

In particular, we will be interested in the norm of the ground and excited states, N_g and N_e,

$$N_g(t)={\rm tr}\{|g\rangle\langle g|\hat{\rho}(t)\}, \tag{2.24}$$

$$N_e(t)={\rm tr}\{|e\rangle\langle e|\hat{\rho}(t)\}, \tag{2.25}$$

the total (system) energy $\langle E\rangle$

$$\langle E\rangle(t)={\rm tr}\{\hat{H}\hat{\rho}(t)\}, \tag{2.26}$$

and the desorption probability $P_{\rm des}$

$$P_{\rm des}(t)={\rm tr}\{\hat{\theta}(Z-Z_d)\hat{\rho}(t)\}. \tag{2.27}$$

Here, $\hat{\theta}(Z-Z_d)$ is a projector in configuration space, with

$$\hat{\theta}(Z-Z_d)=\begin{cases}0, & Z\leqslant Z_d\\ 1, & Z>Z_d\end{cases} \tag{2.28}$$

and Z_d is a point separating adsorbed from desorbed species. In practice, only the ground state (neutral) particles can desorb.

3. Kinetic energy analysis

We are also interested in the kinetic energy distribution of the ground state desorbates. For this purpose we introduce a ''soft projector''

$$\hat{P}_{gg}=\hat{f}(Z)|g\rangle\langle g| \tag{2.29}$$

with $\hat{f}(Z)$ being a Fermi-type cutoff function, which smoothly goes from 0 to 1 with increasing Z

$$\hat{f}(Z)=1-\frac{1}{1+e^{\gamma(Z-Z_d)}}. \tag{2.30}$$

Here, γ is a steepness parameter (see Table I). We define the asymptotic (desorbate) density operator $\hat{\rho}_{gg}^{\mathrm{des}}$ according to

$$\hat{\rho}_{gg}^{\mathrm{des}}=\hat{P}_{gg}^{+}\hat{\rho}\hat{P}_{gg}, \tag{2.31}$$

which in turn can be used to determine the (normalized) kinetic energy of the desorbates according to

$$\langle E_k\rangle(t)=\frac{\mathrm{tr}\{\hat{T}\hat{\rho}_{gg}^{\mathrm{des}}\}}{\mathrm{tr}\{\hat{\rho}_{gg}^{\mathrm{des}}\}}, \tag{2.32}$$

where $\hat{T}=-(\hbar^2/2\mu)(\partial^2/\partial Z^2)$ is the nuclear kinetic energy operator. The reason for choosing a soft projector is in the fact that ρ_{gg}^{des} will be expressed in configuration space representation, and the derivative in Eq. (2.32) will be done by fast Fourier transform (FFT)—see below.

From the kinetic energies also a *translational temperature* T_{trans} can be extracted according to

$$T_{\mathrm{trans}}=\frac{\langle E_k\rangle}{2k_B}. \tag{2.33}$$

4. Probability densities

In passing we note that the diagonal elements of the density matrix in coordinate space can be interpreted as probability densities in direct space (i.e., the probability to find a particle between Z and $Z+dZ$), and the diagonal elements of the Fourier-transformed density matrix are probability densities in reciprocal ($k-$) space (i.e., the probability to find a particle with a momentum between k and $k+dk$).

III. NUMERICAL REALIZATION

A. Time propagation

The Liouville–von Neumann equation (2.5) has, for not explicitly time-dependent problems the formal solution

$$\hat{\rho}(t)=e^{\mathscr{L}t}\hat{\rho}(0). \tag{3.1}$$

For time-dependent problems, we divide the time interval of interest into segments $t_n=n\Delta t$; $n=0,1,2,\ldots$, where Δt is small enough to resolve variations in the Hamiltonian evolution, the dissipation, and the external field. We then express the one-time step propagator, $e^{\mathscr{L}\Delta t}$, which, when acting on $\hat{\rho}(t)$ gives $\hat{\rho}(t+\Delta t)$, as a Newton polynomial of order M[35]

$$e^{\mathscr{L}\Delta t}\approx c_0\mathscr{T}+c_1(\mathscr{L}-z_0\mathscr{T})+c_2(\mathscr{L}-z_1\mathscr{T})(\mathscr{L}-z_0\mathscr{T})+\cdots +c_M(\mathscr{L}-z_{M-1}\mathscr{T})\cdots(\mathscr{L}-z_1\mathscr{T})(\mathscr{L}-z_0\mathscr{T}). \tag{3.2}$$

Here, $\mathscr{T}$ is the identity superoperator, $z_n(n=0,\ldots,M-1)$ are the complex-valued sampling points, and $c_n(n=0,\ldots,M)$ the divided difference coefficients (which contain the time-step Δt and the function values $e^{z_n\Delta t}$ and which can be obtained recursively). The sampling points are complex, because the eigenvalue spectrum of a dissipative Liouvillian is located in the left half of the complex plane [because the Liouvillian is defined as in Eq. (2.5)]. The sampling points are located on a rectangle extending from $-iE_{\max}$ to $+iE_{\max}$ along the imaginary axis, and from 0 to $-W_{\max}$ on the real axis, where $E_{\max}$ is the Hamiltonian and $W_{\max}$ the dissipative energy maximum. The exact location of the z_n is determined with the help of Schwarz–Christoffel conformal mapping,[35] or by the so-called Leja algorithm.[46] The results below make use of Schwarz–Christoffel conformal mapping and the propagation parameters given in Table I.

Note that the expansion (3.2) avoids the prohibitively expensive and memory-consuming diagonalization of a four-index Liouvillian matrix. Rather, only three matrices of dimension $N\times N$ have to be kept in central memory, and only actions of the type $\mathscr{L}\hat{\rho}$ are required.

B. Operator representation

1. General

The evaluation of the operation $\mathscr{L}\hat{\rho}$ calls for a particular representation. In the present application the density is partly unbound—hence we use a configuration space representation, as suggested in Ref. 36. The spatial grid we are employing is of the type

$$Z_i=Z_0+(i-1)\Delta;\quad i=1,2,\ldots,L, \tag{3.3}$$

with the grid parameters defined in Table I.

Unless otherwise noted, general operator matrix elements are henceforth denoted as

$$A_{nm}^{ij}=A_{nm}(Z_i,Z_j) \tag{3.4}$$

(upper indices: grid, lower indices: electronic labels). With this notation, we can calculate the elements of the matrix resulting from the action of the Liouville superoperator on the density $\hat{\rho}$. This gives the change of the density matrix elements at a specified time as

$$\frac{d}{dt}\rho_{nm}^{ij}=(\mathscr{L}\hat{\rho})_{nm}^{ij}=(\mathscr{L}_H\hat{\rho})_{nm}^{ij}+(\mathscr{L}_D\hat{\rho})_{nm}^{ij}. \tag{3.5}$$

2. Hamiltonian part

The action of the Hamiltonian Liouville superoperator $\mathscr{L}_H=-i/\hbar[\hat{H},\bullet]$ on the density matrix $\hat{\rho}$, i.e., the change of the density matrix due to the Hamiltonian evolution, results in

$$(\mathscr{L}_H\hat{\rho})_{gg}^{ij}=T_{gg}^{ij}+(V_g^{ii}-V_g^{jj})\rho_{gg}^{ij}+V_{eg}^{ii}\rho_{eg}^{ij}-V_{eg}^{jj}\rho_{ge}^{ij}, \tag{3.6}$$

$$(\mathscr{L}_H\hat{\rho})_{ge}^{ij}=T_{ge}^{ij}+(V_g^{ii}-V_e^{jj})\rho_{ge}^{ij}+V_{eg}^{ii}\rho_{ee}^{ij}-V_{eg}^{jj}\rho_{gg}^{ij}, \tag{3.7}$$

$$(\mathscr{L}_H\hat{\rho})_{eg}^{ij}=T_{eg}^{ij}+(V_e^{ii}-V_g^{jj})\rho_{ge}^{ij}+V_{eg}^{ii}\rho_{gg}^{ij}-V_{eg}^{jj}\rho_{ee}^{ij}, \tag{3.8}$$

$$(\mathscr{L}_H\hat{\rho})_{ee}^{ij}=T_{ee}^{ij}+(V_e^{ii}-V_e^{jj})\rho_{ee}^{ij}+V_{eg}^{ii}\rho_{ge}^{ij}-V_{eg}^{jj}\rho_{eg}^{ij}, \tag{3.9}$$

where

$$V_n^{ii}=V_n(Z_i), \tag{3.10}$$

$$V_{eg}^{ii}=V_{eg}(Z_i), \tag{3.11}$$

$$T^{ij}_{nm}=(\hat{T}\hat{\rho}-\hat{\rho}\hat{T})^{ij}_{nm}. \tag{3.12}$$

The electric field coupling elements (3.11), for which already $\hat{V}_{eg}=\hat{V}_{ge}$ has been used [see Eq. (2.21)] further simplify under the Condon approximation. Further, the kinetic energy commutator matrix elements T^{ij}_{nm} defined in Eq. (3.12) are calculated by an FFT algorithm, as outlined in Ref. 36.

3. Dissipative part

The matrix elements arising from the action of the dissipative Liouvillian $\mathscr{L}_D$ on $\hat{\rho}$ can be written as a sum of the individual dissipative channel contributions. For the spontaneous emission (quenching) part, we arrive in the general case of coordinate-dependent quenching rates $\hat{\Gamma}_{ge}(Z)$ at the following expressions:

$$(\mathscr{L}_{D1}\hat{\rho})^{ij}_{gg}=\sqrt{\Gamma^{ii}_{ge}}\rho^{ij}_{ee}\sqrt{\Gamma^{jj}_{ge}}, \tag{3.13}$$

$$(\mathscr{L}_{D1}\hat{\rho})^{ij}_{ge}=-\tfrac{1}{2}\rho^{ij}_{ge}\Gamma^{jj}_{ge}, \tag{3.14}$$

$$(\mathscr{L}_{D1}\hat{\rho})^{ij}_{eg}=-\tfrac{1}{2}\rho^{ij}_{eg}\Gamma^{ii}_{ge}, \tag{3.15}$$

$$(\mathscr{L}_{D1}\hat{\rho})^{ij}_{ee}=-\tfrac{1}{2}(\Gamma^{ii}_{ge}+\Gamma^{jj}_{ge})\rho^{ij}_{ee}. \tag{3.16}$$

In deriving Eqs. (3.13)–(3.16), we used the expression (2.14) for the Lindblad quenching operator in the general form (2.8), and introduced successively both the electronic and grid bases. In particular, one has to take the operator nature of the rate in the general case into account, and hence the fact that $\hat{\Gamma}_{ge}$ does not commute with $\hat{\rho}$. As a potential-like entity, the $\hat{\Gamma}_{ge}$ operator is diagonal in the configuration space representation, and therefore the square root operator functions are simply given by

$$\sqrt{\Gamma^{ii}_{ge}}=\sqrt{\Gamma_{ge}(Z_i)}. \tag{3.17}$$

For the indirect excitation step modeled by $\hat{C}_2$ in Eq. (2.16), an analogous procedure leads to

$$(\mathscr{L}_{D2}\hat{\rho})^{ij}_{gg}=-\tfrac{1}{2}[\Gamma^{ii}_{eg}(t)+\Gamma^{jj}_{eg}(t)]\rho^{ij}_{gg}, \tag{3.18}$$

$$(\mathscr{L}_{D2}\hat{\rho})^{ij}_{ge}=-\tfrac{1}{2}\rho^{ij}_{ge}\Gamma^{ii}_{eg}(t), \tag{3.19}$$

$$(\mathscr{L}_{D2}\hat{\rho})^{ij}_{eg}=-\tfrac{1}{2}\rho^{ij}_{eg}\Gamma^{jj}_{eg}(t), \tag{3.20}$$

$$(\mathscr{L}_{D2}\hat{\rho})^{ij}_{ee}=\sqrt{\Gamma^{ii}_{eg}(t)}\rho^{ij}_{gg}\sqrt{\Gamma^{jj}_{eg}(t)}. \tag{3.21}$$

In the special case of coordinate-independent quenching ($\Gamma^{ii}_{ge}=\Gamma_{ge}=$const., i.e., strict exponential resonance decay), and if also the upward rates are idealized as Z-independent [$\Gamma^{ii}_{eg}(t)=\Gamma_{eg}(t)$], Eqs. (3.13)–(3.16) and (3.18)–(3.21) simplify to the analogs of the expressions given in Ref. 31. Then, Eqs. (3.13) and (3.16) describe the loss of the resonance population to the ground state with rate Γ_{ge}, and Eqs. (3.14) and (3.15) the simultaneous decay of the electronic coherences (dephasing) with a rate $\Gamma_{ge}/2$. Analogous interpretations hold for the excitation equations (3.18)–(3.21), except that the transfer and dephasing rates are explicitly time dependent in the DIMET case. Note that, if no direct coupling is operative, the electronic off-diagonal blocks of the density matrix remain zero according to the initial conditions (2.9) or (2.15). Pure electronic dephasing, though not considered here, poses no special additional problem.

A third type of ''dissipative channel'' which is (occasionally) considered here, is connected to the fact that in long-time propagations the density may reach the finite grid boundaries and be reflected. This is avoided by using absorbing boundary conditions at large Z, and an absorbing superoperator of the anticommutator form

$$\mathscr{L}_{D3}\hat{\rho}=[|g\rangle\langle g|\hat{V}_{\rm abs},|g\rangle\langle g|\hat{\rho}]_+ \tag{3.22}$$

with $\hat{V}_{\rm abs}(Z)$ being an absorbing function turning on at large Z,

$$\hat{V}_{\rm abs}(Z)=-\frac{V_0}{\cosh[\beta(Z-Z_e)]} \tag{3.23}$$

and V_0, β, and Z_e being height and steepness parameters and the (large Z) end of the grid, respectively. The matrix elements of the absorber are non-zero only in the (g,g) block, and are given by

$$(\mathscr{L}_{D3}\hat{\rho})^{ij}_{gg}=(V^{ii}_{\rm abs}+V^{jj}_{\rm abs})\rho^{ij}_{gg}. \tag{3.24}$$

Absorbing boundary conditions are not needed on the upper surface, because $\hat{V}_e(Z)$ is strongly bound.

IV. DIET DYNAMICS

A. Estimating a resonance lifetime

We first consider the indirect DIET of NO/Pt(111) within our one-dimensional density matrix model. This section serves not only to gain insight into the characteristic timescales of the process, but also to discuss parameter dependences of the computed observables, and, most importantly, to estimate the lifetime of the resonance state based on experimental data.

The experimental data for NO/Pt(111)[6] we wish to reproduce are the desorption probability per excitation event, and the translational temperature of the desorbing particles. The experimental desorption probability per absorbed photon is 5×10^{-8}. The desorption probability per excitation event is not safely known, but can be estimated to be in the order of $P_{\rm des}\approx10^{-4}$.[6,27] The measured translational temperature is $T_{\rm trans}\approx1200$ K. Within our one-dimensional two-state model, no statement concerning vibrational or spin–orbit excitations can be made.

We first consider the case of a coordinate-independent quenching rate $\hat{\Gamma}_{ge}=\Gamma_{ge}$, and use the potential and other computational parameters defined in Table I. In Fig. 1, snapshots of the nuclear densities (diagonals of the density matrix blocks in coordinate space) as they evolve on the upper and lower surfaces $\hat{V}_e(Z)$ and $\hat{V}_g(Z)$ are shown. The initial state is the Franck–Condon transferred vibrational and electronic ground state (2.9) with $\hat{\sigma}$ given by Eq. (2.11) and $w_v=\delta_{v0}$. A resonance lifetime of $\tau=1/\Gamma_{ge}=2$ fs was assumed. It is seen that the electronically excited adsorbate moves—in an Antoniewicz-like fashion—towards the surface and rapidly looses intensity. Simultaneously, density is created on $|g\rangle$. The major part of the wave packet remains trapped in the ground state chemisorption well. At longer times, however, a

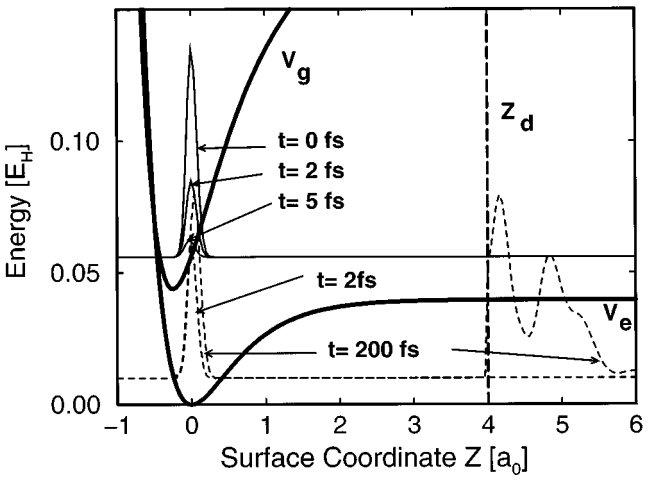

FIG. 1. DIET dynamics with $\tau=2$ fs: snapshots. Shown are the potential curves $\hat{V}_g(Z)$ and $\hat{V}_e(Z)$, the dividing line Z_d separating adsorbates from desorbates, and snapshots of the nuclear density on the upper (thin solid lines) and lower surfaces (thin dashed lines) at various times in the form of $\hat{\rho}_{ee}(Z,Z)$ and $\hat{\rho}_{gg}(Z,Z)$ (arbitrary units for the densities). Since the desorption probability is small, desorbed density has been multiplied by a factor of 50 000 if $Z>Z_a$. The baselines of the nuclear densities are arbitrarily set to 0.056 hartree ($\hat{\rho}_{ee}$) and 0.01 hartree ($\hat{\rho}_{gg}$), respectively.

small fraction of particles is seen to pass the dividing point Z_d separating adsorbed from desorbed species.

In Fig. 2, several computed properties of interest are shown. The upper left panel of the figure, giving the survival probability $N_e(t)$ of the resonance [see Eq. (2.25)], demonstrates the strict exponential continuous decay of the excited intermediate. In the lower left panel it is seen that this decay is accompanied by a decrease in the total system energy $\langle E\rangle$, which falls rapidly from $\langle E\rangle(0)=\langle 0_g|\hat{H}_e|0_g\rangle=57.94\cdot 10^{-3}$ hartree$=1.577$ eV, to a value of 1.84×10^{-3} hartree (0.050 eV) at the largest time considered, $T=500$ fs. This final energy is slightly higher than the pre-excitation system energy $\epsilon_{0g}=\langle 0_g|\hat{H}_g|0_g\rangle$, which is calculated to be $\epsilon_{0g}=1.02\times10^{-3}$ hartree (0.028 eV). Hence, the energy deposited in the molecule–surface bond by an initial impulsive excitation is ca. 1.5 eV, and therefore consistent with inverse photoemission data, which place the center of the $2\pi^*$ resonance of adsorbed NO 1.5 eV above the Fermi level.[37] The absorbed energy is not entirely dissipated—rather, an energy gain of $\Delta\langle E\rangle=\langle E\rangle(T)-\epsilon_{0g}=0.022$ eV is observed.

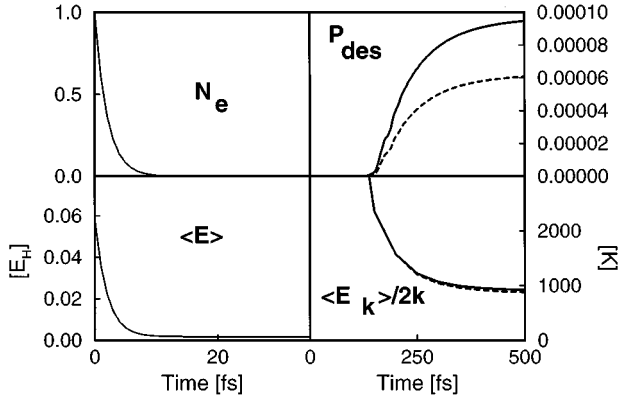

FIG. 2. DIET dynamics with $\tau=2$ fs: properties. Shown are the survival probability on the upper state, N_e [Eq. (2.25)], the total system energy $\langle E\rangle$ [Eq. (2.26)], the desorption probability $P_{\rm des}$ [Eq. (2.27)] and the translational temperature of the desorbates, $T_{\rm trans}$ [Eq. (2.33)], as a function of propagation time. The solid lines are for coordinate-independent quenching, the dashed ones for coordinate-dependent quenching [Eq. (4.1)]. In the left two panels solid and dashed lines are almost indistinguishable.

This tiny energy gain is converted into vibrational excitation of the adsorbate, and an even smaller fraction used to enforce desorption. In Fig. 2, upper right panel, the desorption probability $P_{\rm des}$ is shown as a function of time, as obtained from Eq. (2.27) (solid line). We see that the curve almost saturates at $t=T=500$ fs, and the corresponding asymptotic desorption probability is 0.95×10^{-4}. We consider $P_{\rm des}(T)$ as ''the'' desorption yield (per excitation event) to be compared to the experimental target value of $P_{\rm des}=1\times10^{-4}$. The calculation will predict a few percent higher yields if pushed to longer times. On the other hand, inclusion of vibrational relaxation will tend to decrease $P_{\rm des}$ again. Hence, the agreement between theory and experiment with the choice $\tau=2$ fs is good.

Reasonable agreement between theory and experiment is obtained also for the kinetic energy of the desorbing particles. In Fig. 2, lower right panel, we give the corresponding translational temperatures $T_{\rm trans}$ obtained from Eq. (2.32). It is found that the particles desorb translationally very ''hot,'' and that NO molecules desorbing early have the highest kinetic energy. After $t=T=500$ fs, the translational temperature is $T_{\rm trans}=923$ K, which is reasonably close to the experimental target value of $T_{\rm trans}=1210\pm60$ K.[6]

The question arises of how the agreement obtained is sensitive to (i) the excited state lifetime, (ii) a possible coordinate dependence of the quenching rate, and (iii) the potential parameters. The dependence of the results on the potential parameters has at length been discussed in Ref. 27 (in a wave packet framework, though), and will not further be addressed here. It is sufficient to note that the main conclusions, and in particular the estimate $\tau<5$ fs (see below), remains valid also if (reasonable) parameter variations are allowed for.

The lifetime dependence of both the asymptotic desorption probability $P_{\rm des}(T)$ and the translational desorbate temperature $T_{\rm trans}(T)$ is documented in Table II. An extreme dependence is found for $P_{\rm des}(T)$, which increases from $P_{\rm des}(T)=5.27\times10^{-8}$ for $\tau=1$ fs to $P_{\rm des}(T)=7.24\times10^{-2}$ for $\tau=10$ fs. The dependence of $T_{\rm trans}(T)$ on τ is not so strong, with increasing τ leading to faster free NO molecules. Both observations are consistent with previous wave packet results.[9,10,27] From Table II we conclude that the best agreement with experiment, at least with respect to the desorption yields, is obtained with ultrashort excited state lifetimes in the order of $\tau\approx2$ fs.

B. Coordinate-dependent quenching

To investigate the dependence of the results on the coordinate dependence of the excited state lifetime, an exponential model form for the quenching rate operator has been chosen

TABLE II. DIET dynamics. Time-asymptotic desorption probabilities $P_{\mathrm{des}}(T=500\ \mathrm{fs})$ [Eq. (2.27)] and translational temperatures T_{trans} [Eq. (2.33)] for different coordinate-independent lifetimes τ.

τ (fs)	1	2	3	4	5	10
$P_{\mathrm{des}}(T)$	$5.27\cdot10^{-8}$	$9.47\cdot10^{-5}$	$1.54\cdot10^{-3}$	$6.43\cdot10^{-3}$	$1.50\cdot10^{-2}$	$7.24\cdot10^{-2}$
T_{trans} (K)	635	923	1066	1142	1186	1262

$$\hat{\Gamma}_{ge}(Z)=\Gamma^{0}_{ge}\cdot e^{-\lambda Z}, \tag{4.1}$$

which is consistent which previous theoretical treatments,[9–11,16,27] and which accounts for the fact that electronic quenching close to the surface must be faster than far away from it. The results given so far where for $\Gamma^{0}_{ge}=1/\tau$ and $\lambda=0$. To make a comparison meaningful, we use the parameters $\Gamma^{0}_{ge}=(2\ \mathrm{fs})^{-1}$ and $\lambda=0.5\ a_0^{-1}$ for a coordinate-dependent calculation. This set produces, a resonance decay pattern very similar to the $\Gamma_{ge}=(2\ \mathrm{fs})^{-1}=$const. case. This is demonstrated in the upper left panel of Fig. 2, where the resonance decay is also shown for the coordinate-dependent rate (dashed line). The corresponding curve is almost indistinguishable from the old one, simply because the initial NO wave packet is strongly localized around $Z=0$, where the rate is exactly $(2\ \mathrm{fs})^{-1}$.

Also, the total system energies are strikingly similar (lower left panel of Fig. 2). There is, however, a visible difference in the desorption yield, which decreases by ca. 40%. This observation, which was found in Ref. 27 also, is consistent with the Antoniewicz picture because the coordinate-dependent rate cuts off those parts of the excited state wave packet, which are closer to the surface and which have the best chance to desorb. There is also a small effect of the coordinate dependence on the translational temperature of the desorbates. They become a little colder ($T_{\mathrm{trans}}=882$ K) for the same reason. Both observations suggest to correct the estimated lifetime to be slightly above 2 fs.

In summary, we find that the present one-dimensional DIET model is fairly consistent with experiment if an ultrashort resonance lifetime of $\tau<5$ fs is proposed. We cannot find any huge differences between coordinate-dependent and -independent treatments, or dependences on potential parameters within reasonable domains. Our quantitative estimates are consistent with previous wave packet results,[27] though the lifetime emerging from the density matrix theory is somewhat shorter than in Ref. 27. Unless otherwise noted, below all calculation will be done with an excited state lifetime of 2 fs. (If coordinate-dependent decay rates are used, they will be chosen to resemble a 2 fs resonance decay.)

V. DIMET DYNAMICS

A. General

In Fig. 3 we show several characteristics for a DIMET simulation for NO/Pt(111). To our knowledge, a corresponding experiment has not been performed for this system. Again we use the pure, vibrational and electronic ground state as initial state in Eq. (2.15), corresponding to $T_s=0$ K. Further, the solid curves in Fig. 3 are for coordinate-independent quenching *and* excitation rates, i.e., in Eq. (2.17) we replace $\hat{V}_e(Z)-\hat{V}_g(Z)$ by a constant, $\Delta V=0.056$ hartree (1.5 eV). This constant corresponds to $\hat{V}_e(0)-\hat{V}_g(0)$. For the electronic temperature function we employ the parameters given in Table I, and take $T_m=8000$ K in Eq. (2.18).

As can be seen from the upper left panel in Fig. 3, the assumed parameter set produces a hot-electron profile peaking around ca. 40 fs at a maximum temperature of $T_{\mathrm{max}}=6118$ K, and then falls off on the time scale of a few hundred fs. According to realistic coupled-diffusion simulations for Pd(111), absorbing a 100 fs laser beam (absorbed fluence ca. 5 mJ/cm^2), a temperature profile $T_{\mathrm{el}}(t)$ is produced which is somewhat less peaked than what is assumed here ($T_{\mathrm{max}}\approx5000$ K reached after a few hundred fs, then fall off on a 1–2 ps time scale[11]). Hence, the temperature profile used here rises quite fast (because this allows for a shorter total propagation time), but is otherwise not unrealistic.

With the above approximation the principle of detailed balance leads to the coordinate-independent excitation rate $\Gamma_{eg}(t)$ shown in the middle left panel of Fig. 3 (solid line). Because according to Eq. (2.17) the excitation rate increases *exponentially* with the electronic temperature, the $\Gamma_{eg}(t)$ curve is much more peaked than the $T_{\mathrm{el}}(t)$ curve. Also, $\Gamma_{eg}(t)$ decreases exponentially with the energy difference

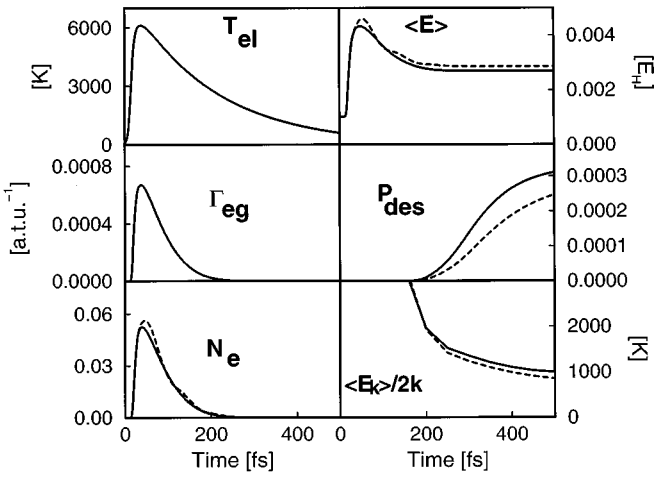

FIG. 3. DIMET dynamics with $\tau=2$ fs and $T_m=8000$ K: properties. Shown are the hot-electron temperature profile $T_{\mathrm{el}}(t)$ [Eq. (2.18)] and the resulting excitation rate $\hat{\Gamma}_{eg}(Z,t)$ [for coordinate-independent quenching, and with the assumption $\Delta V=$const.$=0.056$ hartree in Eq. (2.17)]. Also given are the four properties considered in Fig. 2. For these properties, the solid curves refer to cases where both Γ_{eg} and Γ_{ge} where Z independent, whereas the dashed curves refer to cases where both rates where Z dependent (see the text).

TABLE III. The role of multiple-excitations (τ=2 fs). Shown are the desorption probabilities per excitation event, $P^1_{\rm des}$ [(Eq. 5.2)], as a function of the average number of excitations, $\langle n\rangle$ for various DIMET and DIET simulations. For the DIMET simulations, also the corresponding temperature profile parameters are given.

	DIMET							DIET
T_m (K)	4000	6000	8000	10 000	12 000	14 000	16 000	
$T_{\rm max}$ (K)	3059	4589	6118	7 648	9 176	10 706	12 235	
$\langle n\rangle$	0.087	0.711	2.163	4.268	6.822	9.5915	12.442	1
$P^1_{\rm des}$	$0.90\cdot10^{-4}$	$1.06\cdot10^{-4}$	$1.43\cdot10^{-4}$	$2.19\cdot10^{-4}$	$3.27\cdot10^{-4}$	$4.48\cdot10^{-4}$	$5.70\cdot10^{-4}$	$0.95\cdot10^{-4}$

ΔV; therefore, hot-electron mediated chemistry seems possible only for not too large excitation energies. Further, for systems with several photoactive excited states it seems possible that the lower-lying states may be predominantly hot-electron populated, while the higher ones are accessible only through direct excitation.[47]

The concurring excitation–deexcitation mechanism in the DIMET simulation leads to the resonance-state population curve shown in the lower left panel of Fig. 3 (solid line). In the DIMET simulation, the resonance state never gains a large population. Rather, the N_e curve follows almost instantaneously the $\Gamma_{eg}(t)$ curve, and reaches a maximum at $t\approx50$ fs ($N_e^{\rm max}\approx0.05$). Then, the quenching begins to dominate over excitation.

From the upper right panel of Fig. 3, where the time evolution of the total system energy is shown (solid line), a similar nonmonotonic behavior is seen. The energy first rises due to the fact that the molecule–surface bond absorbs energy from the hot-electron environment, before the energy-consuming quenching takes over. There is, however, asymptotically an energy gain of $\Delta\langle E\rangle=1.67\times10^{-3}$ hartree $=0.045$ eV.

This energy gain is larger than the one found for the DIET process (previous section), and this leads in turn to a larger desorption yield, which asymptotically becomes $P_{\rm des}(T)=3.10\cdot10^{-4}$ in the DIMET case (see middle right panel of Fig. 3, solid curve). It is also observed that the particles are translationally somewhat more excited in the DIMET simulation, where $T_{\rm trans}(T)=997$ K.

Again, the inclusion of effects associated with coordinate-dependent rates are comparatively minor. To demonstrate this, we apply a coordinate-dependent deexcitation rate $\hat\Gamma_{ge}$ (4.1) simulating an (approximate) 2 fs resonance decay, and fully account for all Z dependences in Eq. (2.17). Closer to the surface ($Z<0$), this procedure leads to larger excitation rates than in the coordinate-independent calculation, and for $Z>0$, the excitation rate becomes smaller than previously. The net effects associated with coordinate-dependent excitation and deexcitation rates are small, as can be seen from the corresponding $N_e(t)$, $\langle E\rangle(t)$, $P_{\rm des}(t)$ and $\langle E_k\rangle/2k$ curves (dashed) in Fig. 3. We further find that the approximation $\Delta V=$const. in Eq. (2.17) is of minor importance. Therefore, from now on all calculations will be done with coordinate-independent deexcitation and excitation rates, respectively.

B. Comparison with DIET dynamics

To critically compare DIET with DIMET dynamics, we have to consider that the DIET simulation of the previous section is per excitation event, whereas the DIMET simulation explicitly accounts for the excitation probability. Assuming our target value of 1×10^{-4} is correct, this means that only one among 2000 photons induces the required charge transfer. Hence, the ratio between the calculated DIET and DIMET desorption probabilities is estimated to be $P_{\rm des}^{\rm DIET}/P_{\rm des}^{\rm DIMET}\approx5\times10^{-8}/3.1\times10^{-4}\approx1.6\times10^{-4}$. This clearly demonstrates the superiority of the DIMET over the DIET strategy with respect to desorption yields, as verified experimentally.[6,11]

With the present hot-electron temperature profile, however, we cannot clearly account for the experimental observation that DIMET desorbates have a somewhat lower kinetic energy.[11] Part of this failure is due to numerics: The absolute values of $T_{\rm trans}$ at $T=500$ fs in the DIMET and direct excitation (see below) cases are not converged quite to the same level as in the DIET case. This is because the excitations for those mechanisms are somewhat time delayed [the maximum of $N_e(t)$ is not at $t=0$], and hence the desorption process after 500 fs is not as complete as for the DIET simulation.

More importantly, the translational energies as well as the actual ratio in the desorption yields strongly depend on the particular uv/visible laser characteristics. In particular, one key property of laser-induced desorption is the highly nonlinear dependence of the desorption yield with laser fluence in the DIMET case. In contrast for DIET, due to the uncorrelated nature of the excitations, a linear dependence is observed.[11]

To address this point, we performed a series of DIMET calculations, in which the peak temperature parameter T_m in Eq. (2.17) was varied between $T_m=4000$ and $T_m=16\,000$ K, at otherwise fixed computational parameters. This corresponds to electronic peak temperatures between 3 059 and 12 235 K, respectively (see Table III). In Fig. 4, upper panel, the asymptotic desorption yield $P_{\rm des}(T)$ as a function of the temperature parameter T_m is shown, and a clearly nonlinear behavior observed. If one further assumes, to a first approximation, a linear dependence of the electronic peak temperature on the laser fluence (at otherwise unaffected temperature profile characteristics), this result confirms the experimen-

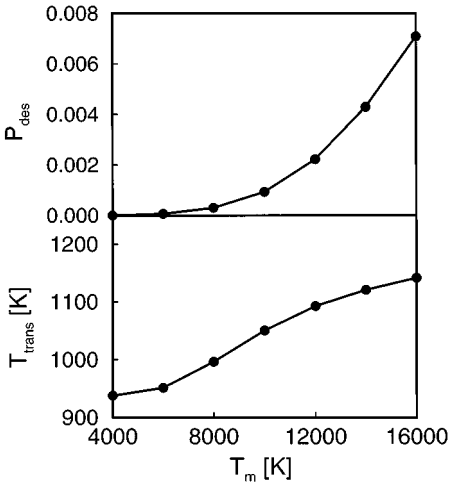

FIG. 4. DIMET dynamics with $\tau=2$ fs. Dependence of desorption probability $P_{\mathrm{des}}(T)$ (upper panel) and translational temperature T_{trans} (lower panel) on the hot-electron peak temperature parameter T_m [Eq. (2.18)].

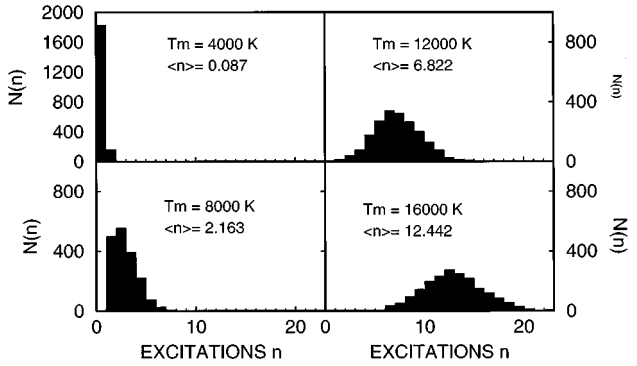

FIG. 5. DIMET dynamics with $\tau=2$ fs. The histograms give (out of a total number of 2000 realizations) the number $N(n)$ of realizations for an n-fold excitation. A kinetic Monte Carlo jump algorithm has been used (see the text). The different panels correspond to different T_m used in Eq. (2.18). $\langle n\rangle$ is the average number of excitations for each case.

tally observed nonlinear increase of the desorption yield with laser fluence in the DIMET case.

Additionally, we find a distinct, monotonic increase of the translational energies of the desorbates with electronic peak temperature (Fig. 4, lower panel). In contrast, the kinetic energy in the uncorrelated DIET model is independent of laser fluence.

C. How many is ''multiple''?

The different outcomes of DIET and DIMET experiments are due to the occurrence of multiple-excitations for the latter.[11] In particular, the higher DIMET desorption yields are a consequence of the fact that an adsorbate, not successful in escaping the well after the first electronic excitation, starts from a vibrationally excited state in the consecutive steps. Since the vibrationally excited wave packet occupies a larger volume of phase space, it better fulfills the Antoniewicz conditions for desorption (see Sec. VII). In the DIET experiment, on the other hand, the (indirect) excitations events are rare and uncorrelated—the adsorbate always starts from its vibrational ground state.

The question arises of how many is multiple? This question can be answered if one utilizes stochastic wave packets rather than (direct) density matrix propagation. As mentioned above, the stochastic wave packet approach[32] is an equivalent alternative to the direct solution of Liouville–von Neumann equations with Lindblad dissipative terms. If the dissipative rates are coordinate independent, the stochastic wave packet approach simply reduces to a jumping wave packet algorithm, and the Gadzuk approach[9,10] is a (deexcitation only) variant of it.[34] If one further is only interested in the quantification of ''multiple,'' and not in the resulting dynamics, the stochastic wave packet algorithm further simplifies to a kinetic Monte Carlo scheme, in which only the bare jumping process is of interest, and in which jump probabilities are proportional to the respective transition rates. Details of this stochastic algorithm are described in Ref. 34.

In Fig. 5, histograms giving the number $N(n)$ of n-fold excitations out of a total number of 2000, as obtained from kinetic Monte Carlo simulations for NO/Pt(111) are shown. In these calculations we once more assumed $\Delta V=$const. $=0.056$ hartree (1.5 eV), and $\tau=2$ fs. The different panels correspond to different T_m used for the hot-electron profile $T_{\mathrm{el}}(t)$ [Eq. (2.18)], at otherwise constant parameters (see Table I). The parameter set underlying Fig. 3 ($T_m=8000$ K, corresponding to $T_{\max}=6118$ K) leads to the lower left panel of Fig. 5. It is found that in this case, the most probable excitation number is $n=2$, but more frequent excitations take place as well. We can define an *average number of excitations* per pulse, $\langle n\rangle$,

$$\langle n\rangle(T_m)=\frac{\Sigma_n n\cdot N(n)}{\Sigma_n N(n)}, \tag{5.1}$$

and we find $\langle n\rangle=2.163$ for $T_m=8000$ K. With $T_m=4000$ K ($T_{\max}=3059$ K), no multiple excitations take place. Rather, most frequently the adsorbate remains unexcited (upper left panel of Fig. 5). It is, however, possible to increase the average number of excitations by increasing the peak temperature, as shown in the right two panels of Fig. 5. At a peak temperature of $T_{\max}=9176$ K ($T_m=12\,000$ K), for example, $n=6$ is the most probable event, and $\langle n\rangle=6.822$. The corresponding distribution becomes broader, and the maximum shift towards higher n, if T_m is further increased (lower left panel of Fig. 5).

It is instructive to define a *desorption probability per excitation event*, P^1_{des}, also for the DIMET case

$$P^1_{\mathrm{des}}(T_m)=\frac{P_{\mathrm{des}}(T;T_m)}{\langle n\rangle(T_m)}. \tag{5.2}$$

Here, $P_{\mathrm{des}}(T;T_m)$ is the density-matrix derived time-asymptotic desorption probability corresponding to a particular choice for T_m, and $\langle n\rangle$ is obtained by the jump algorithm. From Table III we note that the DIMET desorption probabilities $P_{\mathrm{des}}(T;T_m)$ are of the same order of magnitude as the DIET single-excitation result. However, they are not constant. The increase of $P^1_{\mathrm{des}}(T_m)$ with increasing maximum

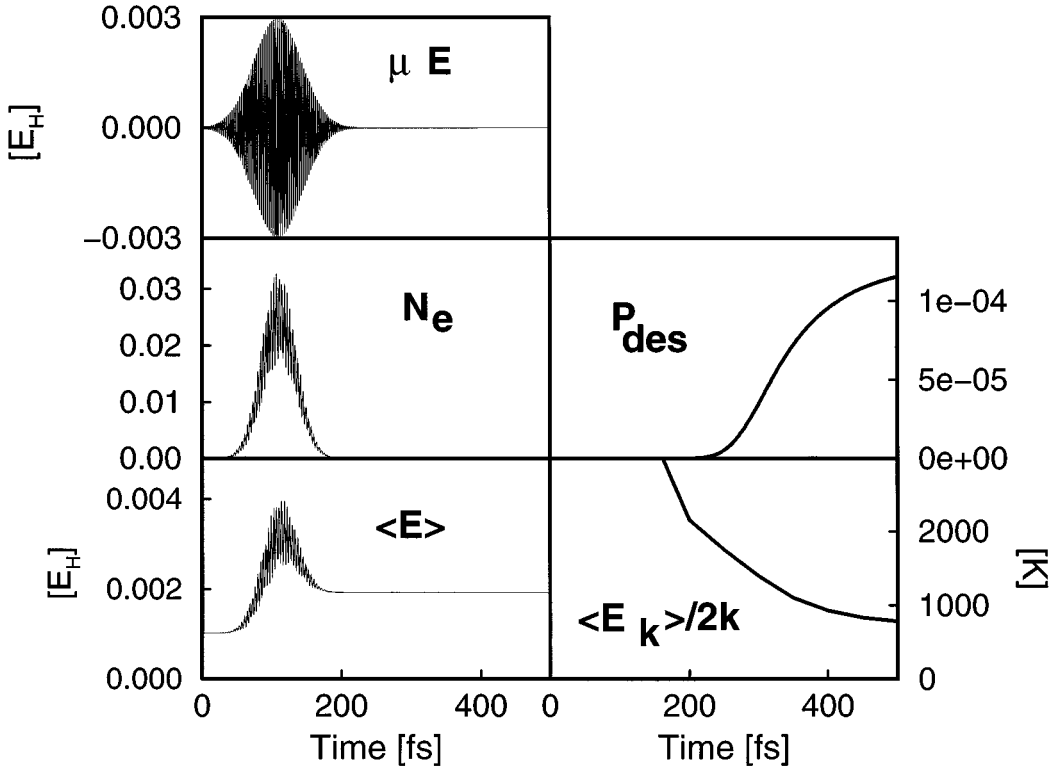

FIG. 6. Direct desorption dynamics with $\tau=2$ fs and field coupling amplitude $\mu_{ge}E_0=0.003$ hartree [Eq. (2.21)]: properties. Shown are the field coupling function $\hat{V}_{eg}(t)=V_{eg}(t)$ [Eq. (2.20), upper left panel], together with the same observables given in Fig. 2.

electronic temperature $T_{\max}$ is to a good approximation linear, and reflects the ''synergetic effects'' associated with the multiple excitations.

VI. DIRECT (DIPOLE) EXCITATION DYNAMICS

Next, a direct dipole excitation scenario along the lines given above is considered. Direct excitation is expected to play a minor role for NO/Pt(111) and for most other metallic substrates, and hence the present simulation has a strong model character.

In Fig. 6 several observables emerging from a simulation with $\tau=2$ fs (coordinate independent) and an electric field coupling amplitude $\mu_{ge}E_0=0.003$ hartree (0.081 eV) [see Eq. (2.21)] are shown. The other field parameters are those of Table I. The laser frequency has been tuned to be approximately in resonance, i.e., $\hbar\omega=0.056$ hartree (1.5 eV). Further, as in the DIMET simulation the initial state was assumed to be vibrationally and electronically unexcited.

With these field parameters, the direct coupling potential becomes the oscillating shape function shown in the upper left panel of Fig. 6. This oscillating field produces a resonance state population $N_e(t)$, which also oscillates in time (middle left panel). Note that, similar to the DIMET case, the maximum population achieved remains small. Also, the total system energy $\langle E\rangle$ is oscillatory, at least as long as the external field is on (lower left panel). There is again a net gain of system energy (0.025 eV), which is partly used for desorption (upper right panel). The desorbates are, for the present set of parameters, colder than in the DIET and DIMET cases [$T_{\text{trans}}(T)=786$ K, lower right panel].

One may also study the scaling of selected observables with laser fluence. We do so by repeating the direct excitation calculation with different field coupling amplitudes $\mu_{ge}E_0$ in Eq. (2.21) in the (realistic) range between 0.001 and 0.007 hartree, at otherwise fixed parameters. In Fig. 7, upper panel, the asymptotic desorption probability $P_{\text{des}}(T)$ is given as a function of the coupling amplitude. We observe a slightly faster than linear increase, more similar to what is expected for an indirect DIET rather than DIMET process (see Fig. 4). Also, at least for the lower field strengths, the translational temperatures of the desorbates are reminiscent to the DIET case, because they only slightly increase with fluence (Fig. 7, lower panel). These results suggest that, with the present field parameters, multiple excitations play only a minor role. It is expected, however, that with larger field amplitudes a multiple-excitation regime becomes accessible, where the desorption probabilities and translational temperatures scale more similarly to the DIMET case. For the highest field strength considered ($\mu_{ge}E_0=0.007$ hartree), the more substantial increase observed for T_{trans} in Fig. 7, already indicates the transition towards a multiple-excitation regime.

Further, the translational temperatures reported in Fig. 7 are systematically lower than for the indirect excitation mechanisms, even for cases where the desorption probability

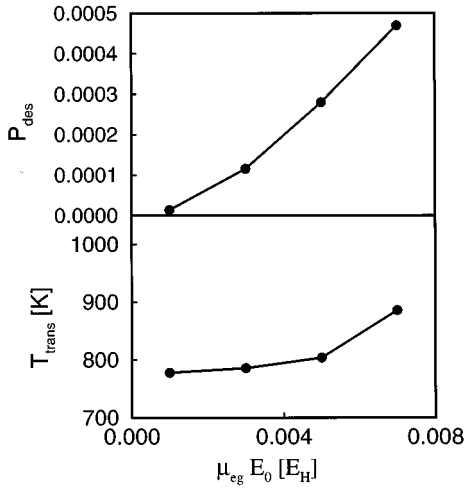

FIG. 7. Direct desorption dynamics with $\tau=2$ fs. Time-asymptotic desorption probability, $P_{\mathrm{des}}(T)$, (upper panel) and translational temperature of the desorbates, T_{trans}, (lower panel) as a function of the field coupling amplitude $\mu_{ge}E_0$ [see Eqs. (2.20) and (2.21)].

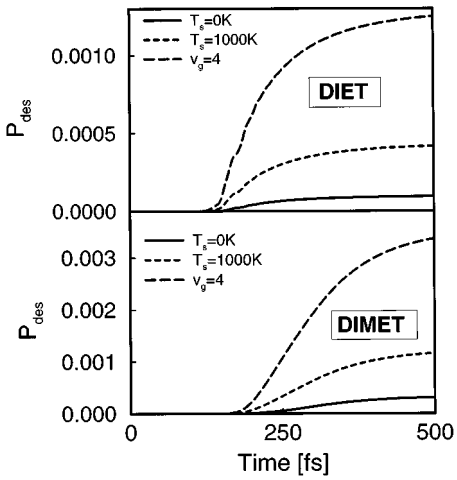

FIG. 8. Controlled photodesorption. Shown is the time dependence of the desorption probabilities, $P_{\mathrm{des}}(t)$, for thermal ($T_s=1000$ K) and nonthermal (vibrational state $v_g=4$) vibrationally prepared adsorbates after indirect DIET (upper panel) or DIMET (lower panel) excitation. The corresponding ''uncontrolled'' simulations ($T_s=0$ K) are shown for comparison.

is comparable. This may be a hint of how to discriminate between direct and indirect excitation mechanisms in experiment.

VII. CONTROL

One major goal of modern quantum molecular dynamics is the active control of chemical reactions. One of various control schemes[48–50] is so-called *vibrationally mediated chemistry* (VMC).[50] If the photoinduced breaking of a particular bond is the reaction of interest, the VMC strategy requires the vibrational preparation of the bond before an uv or visible laser breaks it. If the vibrational excitation is done optically, i.e., by infrared (ir) light, it may be possible to *selectively* break a desired bond, and the corresponding control scheme is called the two-photon ir+uv strategy. If the vibrational preparation of the reactants is done thermally, selectivity is lost but enhanced photodissociation yields may still be achieved.

In connection with photodesorption dynamics, the most important question is whether reaction control, selective or not, is possible even in a strongly dissipative environment. Using wave packet methods we have argued that nonselective[28,30] or selective[29] control of photodesorption is to some extent possible even when strong electronic quenching is present. Here, we will demonstrate the same on the more appropriate density matrix basis. For simplicity, and of obvious relevance for NO/Pt(111), we will restrict ourselves to the hot-electron mediated electronic excitation mechanisms, though the direct electronic excitation scheme itself offers several promising control parameters.

In particular, four different VMC control schemes were considered, depending on whether the NO–surface bond was thermally or ir vibrationally prepared, and whether the subsequent indirect electronic excitation was of the DIET or the DIMET type. The corresponding schemes are:

(1) surface heating, DIET excitation;
(2) surface heating, DIMET excitation;
(3) ir preparation, DIET excitation;
(4) ir preparation, DIMET excitation.

Experimentally, Schemes (1) and (2) correspond to the use of cw and pulsed uv/visible lasers and preheated surfaces (phonon temperature T_s), respectively. Schemes (3) and (4) belong to the ir+uv/visible two-photon family, and again cw or pulsed lasers are used for the electronic excitation. Theoretically, we model these different schemes with the single- and double-dissipative channel models for DIET and DIMET, as described above. The vibrational preparation enters simply through different initial density matrices $\hat{\sigma}$ in Eqs. (2.9) and (2.15), respectively. In the thermal schemes the weights in Eq. (2.11) are the Boltzmann weights given by Eq. (2.13), with the appropriate surface temperatures T_s. The ir experiments are modeled by choosing pure but vibrationally excited initial states with weights of the type (2.12) and with $v=v_g>0$. The latter approach anticipates a selective and complete ir preparation of the molecule–surface bond in a particular vibrational state v_g, i.e., we do not explicitly include the ir electromagnetic field and/or ground state dipole matrix elements. Hence, we do also not distinguish between possible cw and pulsed ir experiments. Further, vibrational relaxation is neglected, i.e., we assume that vibrational relaxation is slow on time scales of vibrational excitation and of the desorption process.

In Fig. 8, the time evolution of the desorption probability is shown for all four cases considered. For comparison, the vibrationally unprepared DIET and DIMET simulations discussed above are also included. Again, the quenching time was assumed to be 2 fs and coordinate independent. Further, the thermal preparation simulations where done for $T_s=1000$ K, and the ir vibrational preparation simulations for vibrational level $v_g=4$.

It is found, as in previous studies, that VMC works also under strongly dissipative conditions. In the DIET case (upper panel of Fig. 8), the thermal preparation increases the asymptotic desorption yield $P_{\mathrm{des}}(T)$ by a factor of $P_{\mathrm{des}}(T_s=1000\ \mathrm{K})/P_{\mathrm{des}}(T_s=0\ \mathrm{K})\approx 4.4$, and the idealized ir preparation scheme leads to approximately 13-fold higher yields. Hence, the two-photon strategy is more successful, as one might expect.

In the DIMET case (lower panel of Fig. 8) the same trend is observed. The DIMET yields are particularly high, because the vibrational preparation occurs in two independent ways, namely (i) through the thermal or ir pathways and (ii) through the electronic multiple excitations, which can also lead to vibrational excited adsorbates in their electronic ground state.[11]

From these studies, though premature due to the idealizations made in connection with the ir preparation and the neglect of vibrational relaxation, we expect clear effects to be seen in possible photodesorption experiments for NO/Pt(111). In particular, the following ''ranking'' for the desorption yields is expected for the different control schemes (1)–(4) introduced above

$$P_{\mathrm{des}}(1)<P_{\mathrm{des}}(3)\approx P_{\mathrm{des}}(2)<P_{\mathrm{des}}(4). \tag{7.1}$$

Further, all ''controlled'' desorption yields are much larger than the uncontrolled ones.

There are also smaller effects to be seen for the translational temperatures of the desorbates. The asymptotic translational temperatures for the four case are $T_{\mathrm{trans}}(1)=1067$ K, $T_{\mathrm{trans}}(2)=1096$ K, $T_{\mathrm{trans}}(3)=1073$ K, and $T_{\mathrm{trans}}(4)=1093$ K. Hence, vibrational preparation tends to produce faster desorbates, and possible differences between DIET and DIMET excitations are somewhat washed out.

VIII. CONCLUSIONS

In conclusion we have shown that a not too unrealistic modeling of bond-breaking processes in a dissipative environment seems possible within density matrix theory. If, as in the present application, (i) the relevant probabilities are small and/or (ii) thermal states are of interest and/or (iii) several different dissipative channels are at work, the direct density matrix propagation scheme is more efficient than stochastic wave packet methods. The inclusion of coordinate-dependent dissipation, and the asymptotic kinetic energy analysis poses no special problem.

In application to the photodesorption model for NO/Pt(111), the following was found:

(1) Experimental DIET desorption yields and translational product energies are suggesting, within a one-dimensional Antoniewicz–Gadzuk two-state model, an ultrashort resonance lifetime of $\tau<5$ fs. Coordinate-dependent quenching does not significantly influence the results; the desorption yields become smaller and the desorbates slower due to the cutting off of the high energy tails of the wave packets.

(2) A dissipative quantum analog of earlier classical studies[11] on the DIMET problem using pulsed lasers has been provided. The nonlinear scaling of DIMET yields with laser fluence is also found for NO/Pt, and traced back to the occurrence of multiple excitations. The notion of multiple can be quantified using a kinetic Monte Carlo algorithm. A significant increase of the desorbate translational energies with laser fluence is observed.

(3) A hypothetical direct excitation scheme is, with respect to desorption yields and translational energies, more reminiscent to the DIET case for the range of field parameters studied here. The products were found to be colder than in the indirect excitation cases.

(4) Controlled photochemistry, employing the concept of ''vibrationally mediated chemistry,'' seems possible also in strongly dissipative environments.

There are several obvious avenues along which the present work can be refined. On the methodological side, the extension of the presented schemes to multidimensions is desirable. On the theoretical modeling side, microscopical quenching models, and the inclusion of vibrational relaxation must be aspired to. Also, a more realistic simulation of the electronic heating and the excitation process in general should be achieved. Urgently, reliable *ab initio* potentials are needed. With respect to applications, the role played by internal adsorbate degrees of freedom during photodesorption, the understanding of other photoprocesses at surfaces, and their active control is of interest. We are presently working along a few of these lines.

ACKNOWLEDGMENTS

Fruitful discussions with Allon Bartana, Eckart Hasselbrink, Jörn Manz, and Martin Wolf are gratefully acknowledged. The Fritz Haber Research Center is supported by the Minerva Gesellschaft für die Forschung, GmbH München, FRG. P.S. acknowledges generous support by the Deutsche Forschungsgemeinschaft (*Schwerpunktprogramm Zeitabhängige Phänomene und Methoden in Quantensystemen der Physik und Chemie* Project No. Sa 547/2-1) R.K. acknowledges the support of the German–Israel Foundation.

[1] S. Holloway, Surf. Sci. **299/300**, 656 (1994).
[2] G. Haase, M. Asscher, and R. Kosloff, J. Chem. Phys. **90**, 3346 (1989).
[3] O. Citri, R. Baer, and R. Kosloff, Surf. Sci. 351, 24 (1996).
[4] X. L. Zhou, X.-Y. Zhu, and J. M. White, Surf. Sci. Rep. **13**, 73 (1991).
[5] F. M. Zimmermann and W. Ho, Surf. Sci. Rep. **22**, 127 (1995).
[6] S. A. Buntin, L. J. Richter, R. R. Cavanagh, and D. S. King, Phys. Rev. Lett. **61**, 1321 (1988); S. A. Buntin, L. J. Richter, D. S. King, and R. R. Cavanagh, J. Chem. Phys. **91**, 6429 (1989).
[7] P. R. Antoniewicz, Phys. Rev. B **21**, 3811 (1980).
[8] D. Menzel and R. Gomer, J. Chem. Phys. **41**, 3311 (1964); P. A. Redhead, Can. J. Phys. **42**, 886 (1964).
[9] J. W. Gadzuk, L. J. Richter, S. A. Buntin, D. S. King, and R. R. Cavanagh, Surf. Sci. **235**, 317 (1990); J. W. Gadzuk, Phys. Rev. B **44**, 13 (1991); J. W. Gadzuk, Surf. Sci. **342**, 345 (1995).
[10] J. W. Gadzuk, in *Femtosecond Chemistry*, edited by J. Manz and L. Wöste (VCH, Weinheim, 1995), Chap. 20.
[11] J. A. Misewich, T. F. Heinz, and D. M. Newns, Phys. Rev. Lett. **68**, 3737 (1992).
[12] E. Hasselbrink, Chem. Phys. Lett. **170**, 329 (1990).
[13] Th. Mull, B. Baumeister, M. Menges, H.-J. Freund, D. Weide, C. Fischer, and P. Andresen, J. Chem. Phys. **96**, 7108 (1992).
[14] T. Hertel, M. Wolf, and G. Ertl, J. Chem. Phys. **102**, 3414 (1995).

[15] E. Hasselbrink, M. Wolf, S. Holloway, and P. Saalfrank, Surf. Sci. (in press).
[16] P. Schuck and W. Brenig, Z. Phys. B **46**, 137 (1982).
[17] J. W. Gadzuk and C. W. Clark, J. Chem. Phys. **91**, 3174 (1989).
[18] W. Brenig, Z. Phys. B **23**, 361 (1976).
[19] K. F. Freed, Surf. Sci. **122**, 317 (1982).
[20] A. R. Burns, E. B. Stechel, and D. R. Jennison, Phys. Rev. Lett. **58**, 250 (1987); E. B. Stechel, D. R. Jennison, and A. R. Burns, in *Desorption Induced by Electronic Transitions, DIET III*, edited by R. H. Stulen and M. L. Knotek (Springer, New York, 1988), pp. 136–143.
[21] A. R. Burns, E. B. Stechel, D. R. Jennison, and Y. S. Li, J. Chem. Phys. **101**, 6318.
[22] Z. W. Gortel, R. Teshima, and H. J. Kreuzer, Phys. Rev. B **37**, 3183 (1988).
[23] S. Harris, S. Holloway, and G. R. Darling, J. Chem. Phys. **102**, 8235 (1995).
[24] H. Guo, Chem. Phys. Lett. **240**, 393 (1995); H. Guo and T. Seideman, J. Chem. Phys. **103**, 9062 (1995).
[25] N. Chakrabarti, V. Balasubramanian, N. Sathyamurthy, and J. W. Gadzuk, Chem. Phys. Lett. **242**, 490 (1995).
[26] Z. W. Gortel, Nucl. Instrum. Methods Phys. Res. B **101**, 11 (1995).
[27] P. Saalfrank, Chem. Phys. **193**, 119 (1995).
[28] C. Daniel, R. de Vivie-Riedle, M.-C. Heitz, J. Manz, and P. Saalfrank, Int. J. Quant. Chem. **57**, 595 (1996).
[29] P. Saalfrank, S. Holloway, and G. R. Darling, J. Chem. Phys. **103**, 6720 (1995).
[30] P. Saalfrank and T. Klamroth, Ber. Bunsenges. Phys. Chem. **99**, 1347 (1995).
[31] P. Saalfrank, R. Baer, and R. Kosloff, Chem. Phys. Lett. **230**, 463 (1994).
[32] R. Dum, P. Zoller, and H. Ritsch, Phys. Rev. A **45**, 4879 (1992); K. Mølmer, Y. Castin, and J. Dalibard, J. Opt. Soc. Am. B **10**, 524 (1993); B. Wolfseder and W. Domcke, Chem. Phys. Lett. **235**, 371 (1995).
[33] G. Lindblad, Commun. Math. Phys. **48**, 119 (1976).
[34] P. Saalfrank, Chem. Phys. (in press).
[35] M. Berman, R. Kosloff, and H. Tal-Ezer, J. Phys. A **25**, 1283 (1992).
[36] M. Berman and R. Kosloff, Comput. Phys. Commun. **63**, 1 (1991).
[37] W. Reimer, Th. Fink, and J. Küppers, Surf. Sci. **193**, 259 (1988).
[38] A. G. Redfield, Adv. Magn. Reson. **48**, 119 (1956).
[39] W. T. Pollard and R. A. Friesner, J. Chem. Phys. **100**, 5054 (1994).
[40] J. Tannor (private communication).
[41] V. Gorini and A. Kossakowski, J. Math. Phys. **17**, 821 (1976).
[42] U. Banin, A. Bartana, S. Ruhmann, and R. Kosloff, J. Chem. Phys. **101**, 8461 (1994).
[43] Ch. Scheurer and P. Saalfrank, Chem. Phys. Lett. **245**, 201 (1995); J. Chem. Phys. **104**, 2869 (1996).
[44] D. M. Newns, T. F. Heinz, and J. A. Misewich, Prog. Theor. Phys. Suppl. **106**, 411 (1991).
[45] C. E. Bartosch, N. S. Gluck, W. Ho, and Z. Ying, Phys. Rev. Lett. **57**, 1425 (1986).
[46] G. Ashkenazi, R. Kosloff, S. Ruhmann, and H. Tal-Ezer, J. Chem. Phys. **103**, 10005 (1995).
[47] E. Hasselbrink (private communication).
[48] D. J. Tannor and S. A. Rice, J. Chem. Phys. **83**, 5013 (1985); D. J. Tannor, R. Kosloff, and S. A. Rice, *ibid*. **85**, 5805 (1986).
[49] P. Brumer and M. Shapiro, Annu. Rev. Phys. Chem. **43**, 257 (1992).
[50] R. V. Ambartzumian, N. V. Chekalin, V. S. Doljikov, V. S. Lethokov, and V. N. Lokhman, Opt. Commun. **18**, 400 (1976); F. F. Crim, Science **249**, 1387 (1990); D. G. Imre and J. Zhang, Chem. Phys. **139**, 89 (1989).